Review

Chinese Science Bulletin

SPECIAL TOPIC
Plasmonics

August 2010 Vol.55 No.24: 2618–2624
doi: 10.1007/s11434-010-4014-6

Advances in the hyperlens

MA ChangBao, AGUINALDO Ryan & LIU ZhaoWei*

Department of Electrical and Computer Engineering, University of California, San Diego, California 92093-0407 USA

Received March 10, 2010; accepted May 10, 2010

As a superlens to overcome the well-known diffraction limit, the hyperlens has received much attention due to its super resolving power and magnifying capabilities. In this article, we review the recent developments, including theoretical and experimental studies on the hyperlens. We also discuss its limitations and potential.

hyperlens, super resolution, microscopy

Citation: Ma C B, Aguinaldo R, Liu Z W. Advances in the hyperlens. Chinese Sci Bull, 2010, 55: 2618–2624, doi: 10.1007/s11434-010-4014-6

The optical microscope is undoubtedly one of the most important tools in the natural sciences. It affords researchers the ability to see, with their own eyes, what was previously not visible to them. However, the resolution of a conventional optical system is limited to approximately half the working wavelength due to the diffraction of light [1,2]. It is beneficial to extend the resolving power of optical microscopy as high as possible. Immersion techniques [3,4] are able to improve the resolution to $\sim\lambda/(2n)$, which, however, is limited by the low refractive index n of natural materials. In 2000, Pendry proposed that a material with a negative refractive index, which was originally discussed by Veselago [5], could enable the realization of a perfect lens [6]. The operation of Pendry's perfect lens lies in the ability of a negative index slab to couple and amplify the evanescent waves carrying high spatial frequency information. This idea has stimulated the emergence of a number of superlenses with resolving powers beyond the diffraction limit [7–17], among which the hyperlens [12,13,18] has attracted much attention due to its ability to send an image of a deep sub-wavelength object to the far field. Our purpose in this paper is to review the recent theoretical and experimental developments of the hyperlens. We will start with the theory, followed by an experimental demonstration of the optical hyperlens, and then introduce an acoustic hyperlens [19]. Finally, we will discuss the limitations and potential of the hyperlens.

1 Theory

The original proposal for a hyperlens was conceived independently by two separate groups [12,18]. The impetus for proposing the hyperlens is the desire to push optical microscopy beyond the diffraction limit. The most ideal scheme, shown in Figure 1(a), is to integrate the novel device into an otherwise conventional microscope. Fundamentally, what is needed is the compression of the angular spectrum of a diffracted field such that a sufficient amount of the evanescent information is compressed into the passband of the microscope's transfer function, as shown in Figure 1(b). Using the same fundamental theory of operation, both groups aimed to solve the problem of far-field imaging beyond classic diffraction. The first group, however, explored the ideas of both planar and curved surfaces ultimately yielding to the curved geometries as a way to circumvent the possibility of asymmetric losses being incurred in the imaging of different portions of an extended image [18]. This account of the operating theory is terse and guided by physical intuition and is confirmed by finite element method (FEM) simulations. The proposal of the second group, in which the term 'hyperlens' was actually

*Corresponding author (email: zhaowei@ece.ucsd.edu)

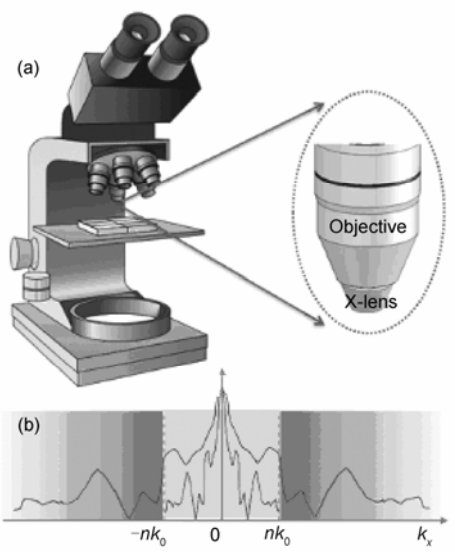

Figure 1 (a) To extend the use of optical microscopy beyond the diffraction limit in a practical manner, a novel "X-lens" should be simply integrated into an otherwise conventional microscope. (b) In terms of the angular spectra of imaged fields, the diffraction limit arises from the loss of evanescent information that falls outside the passband (width of $2nk_0$) of the microscope. If the angular spectrum can be compressed to satisfactorily fit through the passband (i.e. the compression of evanescent fields into propagating waves), the image can be resolved.

coined, concentrates on the curved surfaces appearing in a cylindrically symmetric geometry and expounds on the fundamental theory of why and how a hyperlens works [12]. Additional work by this group led to a ray optics approach to the understanding of the hyperlens [20].

The fundamental principle, governing the ability of the hyperlens to resolve images beyond the diffraction limit, is in the use of a metamaterial with a hyperbolic dispersion relation; hence the term 'hyperlens' [12]. Considering a cylindrical coordinate system (r, φ, z) with no z-variation and an anisotropic permittivity, the dispersion relation of an electromagnetic wave can be written as

$$\frac{k_r^2}{\varepsilon_\varphi}+\frac{k_\varphi^2}{\varepsilon_r}=\frac{\omega^2}{c^2}, \tag{1}$$

where k_r and k_φ are the wave vectors and ε_r and ε_φ are the electric permittivities in the r and φ directions, respectively; ω is the circular frequency and c is the velocity of light. For common dielectrics (i.e. materials which exhibit positive real permittivities), this equation is that of an ellipse. Thus, the total wave vector of an electromagnetic wave at a given frequency is bound to the perimeter of this ellipse, as shown by the short-dashed curve in Figure 2(a) for $\varepsilon_\varphi = \varepsilon_r$ (i.e. a circle). This condition on the magnitude of the wave vector places an intrinsic limit on the spatial frequencies that a traditional lens may resolve. Considering eq. (1) under the condition $\varepsilon_\varphi > 0$ and $\varepsilon_r < 0$, a hyperbolic dispersion relation result is shown by the solid curve in Figure 2(a). That is to say, the iso-frequency curve of the k_r-k_φ plot becomes a hyperbola yielding an unbound value of the magnitude of the wave vector. It is therefore plausible that such a material system can be used to fabricate a lens capable of arbitrarily imaging high spatial frequencies, thus surpassing the diffraction limit. Due to the relatively unusual conditions of the permittivity components, it is necessary that the hyperlens be made of a metamaterial. It is worth noting that such metamaterials possessing dielectric anisotropy of differing signs are now known as indefinite media [21].

A cylindrical geometry was proposed for the hyperlens based on the fact that real materials will exhibit a certain degree of loss. Although it is possible to realize hyperlens imaging with an asymmetric design, a consequence of the material loss is that two rays, originating at different points on the input plane and thus traversing different path lengths to the output plane, will suffer different amounts of attenuation and spatial broadening [18]. This would lead to distortion and loss of fidelity in the final image. A cylindrical hyperlens circumvents this problem by having all rays originating from the input plane (the inner surface in Figure 2(b)–(d)) travel equal path lengths through the metamaterial. In this geometry, the compression of the φ-component of the wave vector transforms evanescent portions of the angular spectrum into resolvable information and the magnification at the output surface is given simply by the ratio of the radii at the two surfaces $r_{\text{outter}}/r_{\text{inner}}$ [12,18].

FEM simulations representative of the operation of the hyperlens are shown in Figure 2(c) and (d). Figure 2(b) shows the optical field distribution in an ordinary material due to two point sources separated by a sub-wavelength distance; clearly, the image of two separate sources is irresolvable in the far field. By placing the two sub-wavelength separated point sources in close proximity to the inner surface of the hyperlens, as shown in Figure 2(c), the optical field distribution yields an image of the two sources in the far field. It is also interesting to note that the hyperbolic dispersion may not be strictly necessary; this may be beneficial for practical reasons when fabricating the metamaterial hyperlens. Because the purpose of the hyperbolic dispersion is to access large components of the tangential wave vector, the same access can be achieved using high eccentricity elliptic dispersion (long-dashed curve in Figure 2(a)). The corresponding field simulation is shown in Figure 2(d); similar far field imaging of a sub-wavelength feature is realized and is similar to, but not as good as, the hyperbolic case of Figure 2(c).

Additional theory regarding the ray optics of the cylindrical hyperlens was developed based on the eikonal/Hamiltonian approach [20]. A major result of this study is the understanding of the profound scattering that occurs due to a combination of rays following a spiral-like path through the hyperlens and the large reflections at the hyperlens surfaces, as shown in Figure 3(a). Indeed, this is not completely surprising since the hyperlens design calls for

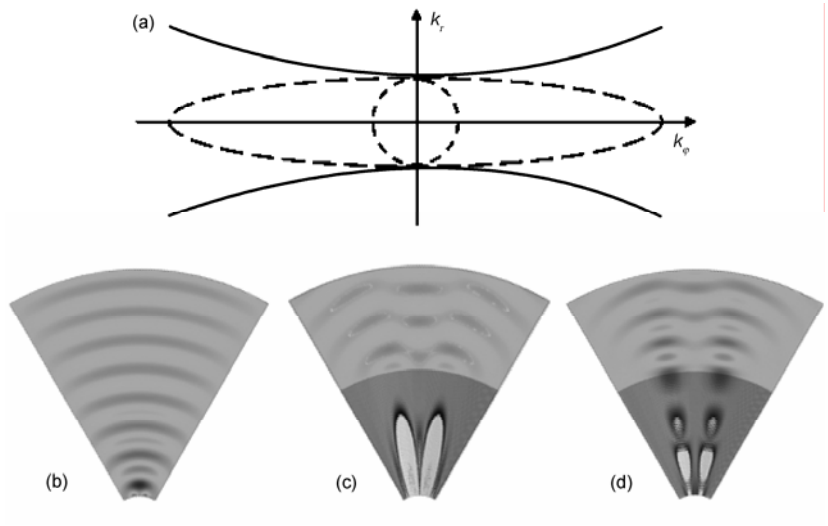

Figure 2 (a) Isofrequency dispersion contours indicating circular ($\varepsilon_\varphi = \varepsilon_r > 0$), elliptical ($0 < \varepsilon_\varphi \neq \varepsilon_r > 0$), and hyperbolic ($\varepsilon_\varphi > 0$, $\varepsilon_r < 0$) behavior. (b)–(d) Simulated field distributions arising from two point sources spaced at a sub-wavelength distance. (b) Field plot showing that the two separate sources cannot be imaged under ordinary circumstances. (c) When placed at the input of the hyperlens (with a hyperbolic dispersion), however, information distinguishing the two point sources propagates to the far field. (d) When using a metamaterial that exhibits a highly eccentric elliptical dispersion, a similar super resolution imaging is observed but with degraded image fidelity.

strong anisotropy in the metamaterial permittivity. Strong scattering can obviously be a detrimental effect in imaging applications; therefore, design rules have been proposed to impedance match the hyperlens metamaterial with the medium it is immersed in, thus reducing the surface reflections [22]. These rules have been derived through a transformation optics approach [23], in which the field inside the inner radius of the hyperlens is concentrically mapped into the hyperlens itself. The most ideal design rules are, however, not practical in an experimental sense due to the precise control needed over both the metamaterial permittivity and permeability. It is also not necessarily reasonable to design a magnetic metamaterial in the optical regime. Therefore, relaxed design rules allowing for non-permeable metamaterials have also been presented. The trade-off with these relaxed rules is that impedance matching may only occur at one of the hyperlens surfaces instead of both. This trade-off is not detrimental as can be seen in Figure 3(b), in which the imaged field distribution is compared in the cases of impedance matching at either the inner or outer surface or both. Simulated field distributions throughout the hyperlens show the effects of the impedance matching of only the outer (Figure 3(c)) or the inner (Figure 3(d)) surface.

The cylindrical hyperlens design may not be convenient in its use of curved surfaces. Indeed, in microscopy it is usually the case that the specimen under observation lies on a plane. Furthermore, if the hyperlens were to be included as an addition to the conventional microscope, then it would make sense that the output surface is also planar. Such designs have been shown to be theoretically feasible via transformation optics [24,25]. In such designs, the metamaterial properties are designed to bend light rays emanating from sub-wavelength features in such a way as to provide

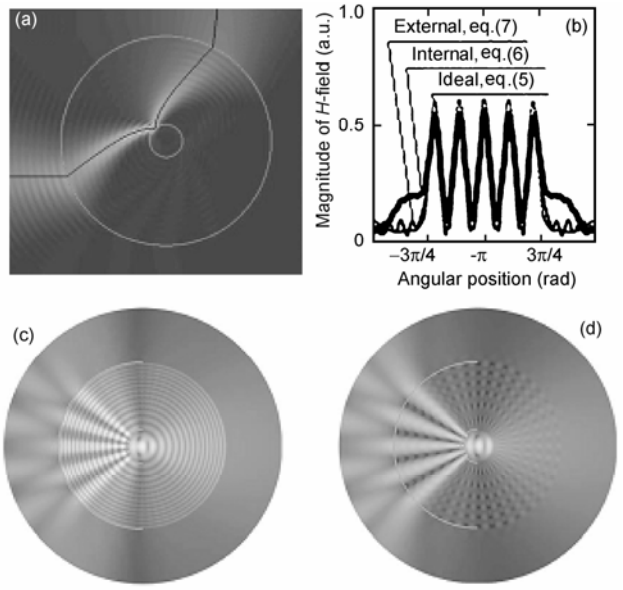

Figure 3 (a) Scattering effect of the hyperlens due to high reflections; an incident beam from the left side is scattered after it encounters the inner surface of the hyperlens. (b) Output surface field distributions for five sub-wavelength spaced point sources under conditions of impedance matching at the external surface only, the internal surface only, and at both surfaces (ideal). Two-dimensional field plots are also shown for the internal (c) and external (d) matching conditions. Reprinted with permission from [20,22].

for a magnified, resolvable image on a flat output plane. One such approach is to take a portion of the cylindrical hyperlens and have it embedded in a metamaterial slab [25]. The design transforms the cylindrical domain of the hyperlens onto a planar surface. This design has been shown to operate even when the material is truncated at its sides thus

being more than adequate for ready integration. The other design makes use of planar surfaces at both the input and output surfaces [24], as shown in Figure 4. Such a design uses coordinate transforms between regions I and II where the interfaces of the alternating layers in Figure 4(a) correspond to the *u* axis and the lines correspond to the *v* axis. The design is such that light rays traverse along the *v* axis, as shown in Figure 4(b). It should be emphasized that these designs are different from a truncated cylindrical hyperlens [26] or a completely planar hyperlens [18]. In the former, the cylindrical output surface is mechanically planarized; in the latter, no optical transformation is performed (i.e. a Cartesian coordinate system suffices) and asymmetric losses occur. Clearly, the transformation optics approach would yield a higher degree of image fidelity.

2 Experimental demonstration

The first optical hyperlens [13] was successfully fabricated using the conformal film deposition method on a half-cylindrical cavity on a quartz substrate, as shown in Figure 5(b). It consisted of 16 pairs of layers composed of 35-nm-thick silver and 35-nm-thick alumina, above which a 50-nm-thick chromium layer was deposited to block the unwanted incident light. To test this hyperlens, subdiffraction limited objects were fabricated on the chrome layer. A plane wave at the wavelength of 365 nm was used to illuminate the objects. Based on the designed metamaterial properties, the scattered light (evanescent wave) by the objects that possessed high transverse *k*-vectors could be collected by the hyperlens and continue to propagate outwards along the radial direction. During the propagation, the high transverse *k*-vectors were compressed gradually, resulting in a magnified image of the subdiffraction limited object on the outer boundary of the hyperlens. The *k*-vector of the image on the outer boundary was compressed small enough to propagate in the medium surrounding the outer boundary of hyperlens, so the image could continue to propagate and thus be detected with conventional optics in the far field. By combining this hyperlens with a conventional microscope, as schematically shown in Figure 5(a), a pair of 35 nm wide lines, separated by 130 nm, were directly resolved in the far field without data processing for image reconstruction, attaining a magnification of 2.3. Figure 5(c) and (d) show the comparison of the images acquired with and without the hyperlens. It can be easily seen that without the hyperlens, the sub-diffraction limited object could not be resolved. Besides this hyperlens, another cylindrical type of magnifying superlens consisting of concentric alternate PMMA and vacuum rings on a gold film was also demonstrated at the wavelength of 515 nm [10].

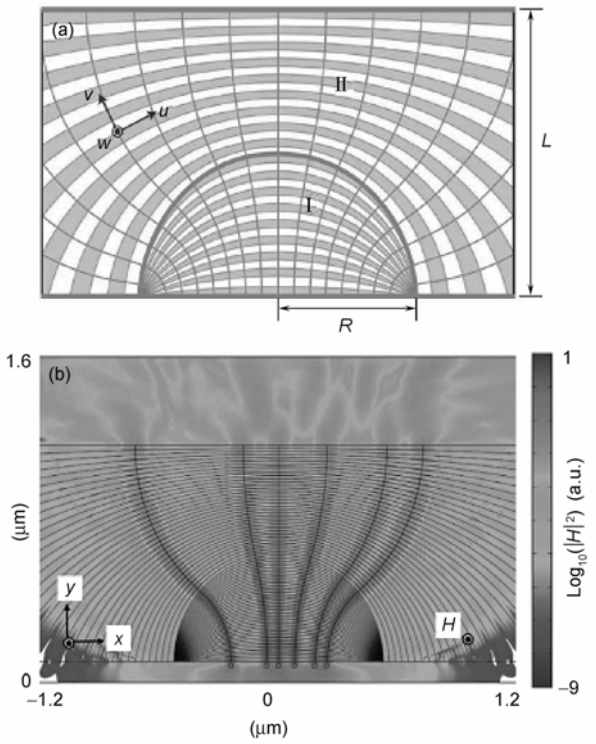

Figure 4 Transformation optics approach to the design of a hyperlens with flat input and output surfaces. (a) Alternating layers of appropriate metal and dielectric, plus the designed geometry, give rise to a metamaterial in which rays of light propagate along the blue lines. (b) Simulated field distribution of six sub-wavelength spaced point sources that can be resolved with this design. Reprinted with permission from [24].

These initial proof-of-concept experiments were demonstrated at a UV (365 nm) wavelength. It would be useful to move the working wavelength to cover the entire visible light band, and thus enable a broad range of applications, such as the study of live cells and molecules. Smith et al. systematically investigated the metamaterial optical hyperlens for this purpose [27,28]. Two different material systems, Al_2O_3/Ag and TiO_2/Ag, were investigated for the visible band for oxide:metal volume ratios ranging from 0 to 6. A picture clearly showing what material combination and wavelength can be used for designing a VIS hyperlens was obtained and shown in Figure 6. As is discussed in the theory section above, a highly anisotropic elliptically dispersive material can also support the transmission of high spatial frequency information, although the wave vector is not unbounded as in a hyperbolically dispersive material. The data in the elliptic dispersion regime with higher oxide:metal ratios for hyperlens purposes is also included in Figure 6. Note that the dashed and dotted curves are the impedance matching modes of the hyperlens for the surrounding water and air. That is, a hyperlens configuration on these impedance matching curves satisfies $\mathrm{Re}(\sqrt{\varepsilon_\varphi}) = n_{\mathrm{medium}}$, so reflections can be avoided at the outer interface of the hyperlens. Here n_{medium} is the refractive index of the medium that the hyperlens is immersed in.

Using a different material system (In)GaAs/Ag and the roll-up technique, Schwaiger et al. fabricated multilayer

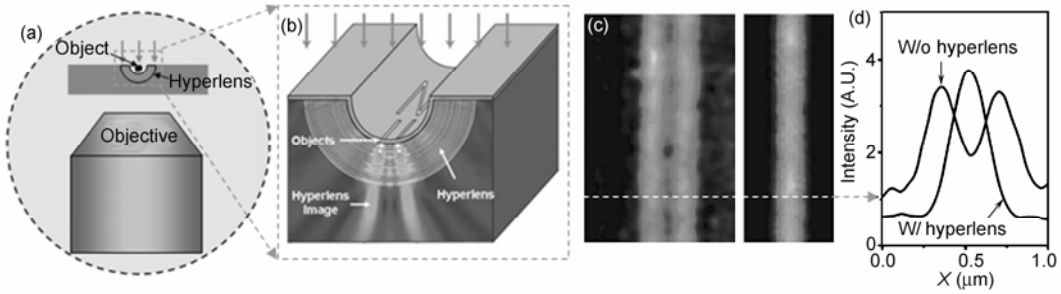

Figure 5 An experimental demonstration of the first optical hyperlens. (a) Schematic of the experimental setup combining a hyperlens with a conventional microscope. (b) Hyperlens with sub-diffraction limited object. (c) Images of the sub-diffraction limited object obtained with (left) and without (right) the hyperlens. (d) Intensity profile of a cutline on the images in (c). Reprinted with permission from [11].

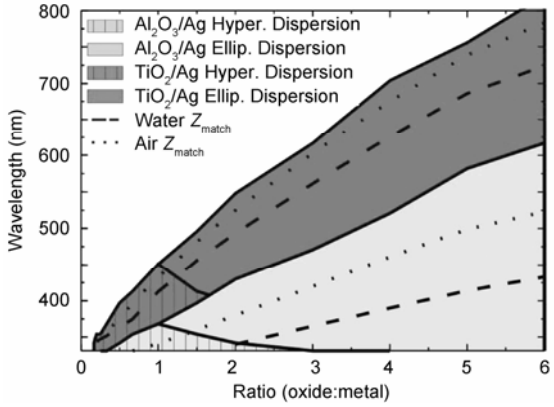

Figure 6 Tunable dispersion range of Al_2O_3/Ag and TiO_2/Ag for hyperlensing effects. Reprinted with permission from [27,28].

tubes and measured the transmission though the tube walls using two point sources on a metalized fiber taper [29]. Their experimental results show that the plasma frequency of the multilayer tubes can be tuned over a broad range in the visible and near infrared by varying the volume ratio of the materials. Further numerical study shows that the transmission through the multilayered wall of the tube is actually a hyperlensing effect.

3 Acoustic hyperlens

While the hyperlens concept was proposed and demonstrated for electromagnetic waves at optical frequencies, it can also be applied to overcome the diffraction limit of acoustic waves. Li et al. experimentally demonstrated, for the first time, an acoustic magnifying hyperlens using a non-resonant radially symmetric layered brass structure [19]. The principle of an acoustic hyperlens is to tune the anisotropic effective mass density to allow for the transmission of high transverse acoustic wave vectors, mimicking hyperlensing action, and thus achieve super resolution. As shown in Figure 7(a), the acoustic hyperlens consists of 36 brass fins arranged in a 180° sectorial shape. Each fin is 19.1 cm long, extending from an inner radius of 2.7 cm to the outer radius of 21.8 cm. The fins are 3 mm thick and subtend an angle of 2.5°. Between two adjacent fins is an air gap also subtending 2.5°, resulting in a volume filling factor of 0.5. The acoustic hyperlens was tested with two in-phase sound sources of 1 cm diameter and 1.2 cm separation. Frequencies were swept from 4.2 to 7.0 kHz using the pressure mapping method. These two sub-wavelength sources in front of the inner surface of the acoustic hyperlens were successfully resolved at the outer surface of the hyperlens. The experimentally measured pressure profile in the output space is shown in Figure 7(b), and the simulated pressure field that matches the experimental results well is shown Figure 7(c). Because there are no resonant structures [30] in this acoustic hyperlens design, it can work in a broad band of acoustic frequencies. Therefore, the acoustic hyper-

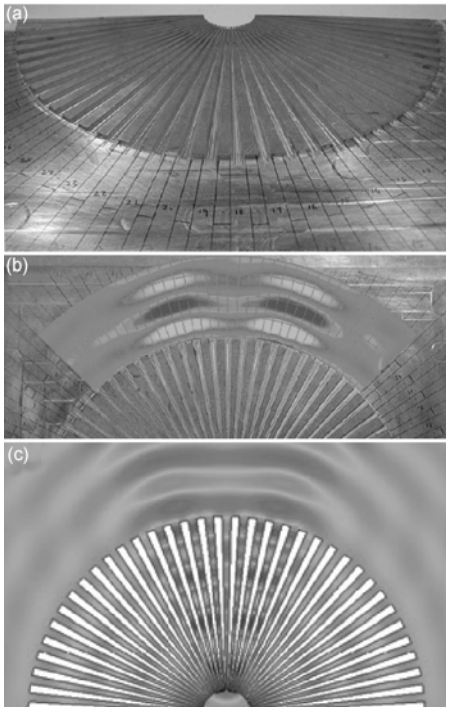

Figure 7 (a) Acoustic hyperlens. (b) Experimentally measured pressure profile in the output space of the acoustic hyperlens. (c) Simulated pressure field. Reprinted with permission from [19].

lens concept may be extended to a number of applications where electromagnetic wave detection may have difficulties such as *in utero* imaging, underwater detection, etc.

The acoustic hyperlens term stems from the optical hyperlens concept, of which the metamaterial dispersion may be either a highly anisotropic hyperbola or ellipse. The models of the two types of hyperlenses differ in some aspects because an electromagnetic wave is transverse and an acoustic wave is longitudinal. The comparisons of the two hyperlens models are summarized in Table 1. The acoustic hyperlens demonstrated has only positive effective densities, so its dispersion is a highly eccentric ellipse, due to its much larger angular effective density ρ_φ compared with the radial effective density ρ_r. As a result, acoustic waves with high transverse momentum carrying sub-diffraction limited information of the acoustic object can propagate in the hyperlens and thus an image with sub-diffraction limited resolution can be obtained.

4 Outlook

The demonstrated hyperlenses have achieved, although moderately, subdiffraction limited resolution with optical and acoustic waves. The performance of a hyperlens can be further improved several times by optimization, in which the geometry, material loss and fabrication play important roles, and can be extended to other electromagnetic wave frequency bands such as microwave and THz. One limitation of the hyperlens imaging is that the object has to be placed very close to the inner surface of the hyperlens, which physically limits the imaging depth and field of view. From this point of view, the applications of the hyperlens should be focused on 2D surface imaging which is similar to total internal refraction (TIR) microscopy. In addition, so far the demonstrated hyperlenses are based on cylindrical geometries, which can only achieve super resolution in one direction. Thus, three-dimensional spherical hyperlenses with super resolution in all transverse directions are desired for realistic applications. An example of a spherical hyperlens is shown schematically in Figure 8, which consists of multilayered half spheres of metal and dielectric materials.

The hyperlens demonstrations have sparked the pursuit of subdiffraction limited resolution in the far field, so that an image of the object with super resolution can be obtained directly in the far field, without time-consuming point-by-point scanning and image reconstruction. This enables the reciprocal usage of the hyperlens with an object in the far field of outer space for photolithography which specifically demands super resolution. Therefore, hyperlenses may find application in various areas, such as super resolution imaging, nano-manufacturing [26], sensing [29] and data storage. We finally note that a hyperlens actually works in a projection manner, i.e. plane to plane mapping, between its

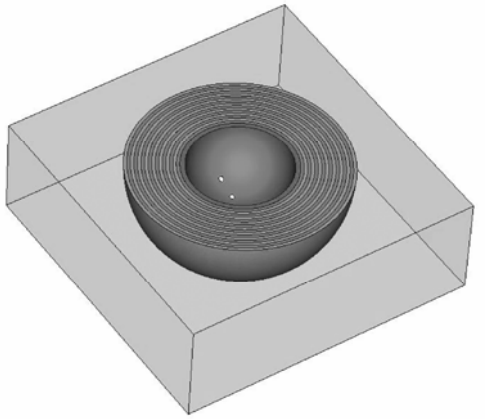

Figure 8 Schematic of three-dimensional spherical hyperlens.

Table 1 Comparison of the optical and acoustic hyperlens models

	Optical hyperlens	Acoustic hyperlens	Common parameters
Dispersion	Hyperbolic or elliptic: $\frac{k_r^2}{\varepsilon_\varphi}+\frac{k_\varphi^2}{\varepsilon_r}=\left(\frac{\omega}{c}\right)^2$ · ε_r and ε_φ are the effective permittivities in the radial and angular directions · c is the velocity of light in vacuum · Condition: $\lvert\varepsilon_r\rvert >> \varepsilon_\varphi$	Elliptic: $\frac{k_r^2}{\rho_r}+\frac{k_\varphi^2}{\rho_\varphi}=\frac{\omega^2}{B}$ · ρ_r and ρ_φ are the effective densities in the radial and angular directions, respectively · B is the effective bulk modulus · Condition: $\varepsilon_r >> \varepsilon_\varphi$	· k_r and k_φ are wave vectors in the radial and angular directions · ω is the circular frequency
Effective media theory	$\varepsilon_\varphi = p\varepsilon_m + (1-p)\varepsilon_d$ $\varepsilon_r = \frac{\varepsilon_m\varepsilon_d}{(1-p)\varepsilon_m + p\varepsilon_m}$ ε_m and ε_d are the permittivity of the metal and dielectric constructing the metamaterials	$\rho_\varphi = p\rho_1 + (1-p)\rho_2$ $\rho_r = \frac{\rho_1\rho_2}{(1-p)\rho_1 + p\rho_2}$ $B = \frac{B_1B_2}{(1-p)B_1 + pB_2}$ ρ_1 and ρ_2 are the density, and B_1 and B_2 are the bulk modulus of the metal and the filing material	p is the volume filling factor of metal

inner and outer interfaces. Thus, a hyperlens cannot focus a plane wave to a spot, i.e. a hyperlens lacks the function of the Fourier transform, which is one of the fundamental functions of a conventional optical lens. This may limit its capability in information processing in Fourier space. We anticipate that superlenses with a Fourier transform function and other basic properties of a conventional optical lens, such as focusing, imaging and collimating, would emerge and thus work like a conventional optical lens in addition to its super resolving power.

1 Abbe E. Beitrage zur Theorie des mikroskops und der mikroskopischen wahrnehmung. Arch Mikroskop Anat, 1873, 9: 413–420
2 Rayleigh L. On the theory of optical images with special reference to the optical microscope. Phil Mag, 1896, 5: 167–195
3 Kino G. The solid immersion lens. Proc SPIE, 1999, 3740: 2–6
4 Rothschild M, Bloomstein T M, Kunz R R, et al. Liquid immersion lithography: Why, how, and when? J Vac Sci Technol B, 2004, 22: 2877–2881
5 Veselago V G. The electrodynamics of substances with simultaneously negative values of ε and μ. Sov Phys Usp, 1968, 10: 509–514
6 Pendry J B. Negative refraction makes a perfect lens. Phys Rev Lett, 2000, 85: 3966–3969
7 Fang N, Lee H, Sun C, et al. Sub-diffraction-limited optical imaging with a silver superlens. Science, 2005, 308: 534–537
8 Taubner T, Korobkin D, Urzhumov Y, et al. Near-field microscopy through a SiC superlens. Science, 2006, 313: 1595
9 Salandrino A, Engheta N. Far-field subdiffraction optical microscopy using metamaterial crystals: Theory and simulations. Phys Rev B, 2005, 74: 075103
10 Smolyaninov I, Hung Y, Davis C. Magnifying superlens in the visible frequency range. Science, 2007, 315: 1699–1701
11 Zhang X, Liu Z. Superlenses to overcome the diffraction limit. Nat Mater, 2008, 7: 435–441
12 Jacob Z, Alekseyev L, Narimanov E. Optical hyperlens: Far-field imaging beyond the diffraction limit. Opt Express, 2006, 14: 8247–8256
13 Liu Z, Lee H, Xiong Y, et al. Far-field optical hyperlens magnifying sub-diffraction-limited objects. Science, 2007, 315: 1686
14 Smith D R, Pendry J B, Wiltshire M C K. Metamaterials and negative refractive index. Science, 2004, 305: 788–792
15 Vedantam S, Lee H, Tang J, et al. A plasmonic dimple lens for nanoscale focusing of light. Nano Lett, 2009, 9: 3447–3452
16 Verslegers L, Catrysse P B, Yu Z, et al. Deep-sub-wavelength focusing and steering of light in an aperiodic metallic waveguide array. Phys Rev Lett, 2009, 103: 033902
17 Ma C, Liu Z. Focusing light into deep sub-wavelength using metamaterial immersion lenses. Opt Express 2010, 18: 4838–4844
18 Salandrino A, Engheta N. Far-field subdiffraction optical microscopy using metamaterial crystals: Theory and simulations. Phys Rev B, 2006, 74: 075103
19 Li J, Fok L, Yin X, et al. Experimental demonstration of an acoustic magnifying hyperlens. Nat Mater, 2009, 8: 931–934
20 Jacob Z, Alekseyev L, Narimanov E. Semiclassical theory of the hyperlens. J Opt Soc Am A, 2007, 24: A52–A59
21 Smith D R, Schurig D. Electromagnetic wave propagation in media with indefinite permittivity and permeability tensors. Phys Rev Lett, 2003, 90: 077405
22 Kildishev A, Narimanov E. Impedance-matched hyperlens. Opt Lett, 2007, 32: 3432–3434
23 Driscoll T, Basov D N, Starr A F, et al. Free-space microwave focusing by a negative-index gradient lens. Appl Phys Lett, 2006, 88: 081101
24 Han S, Xiong Y, Genov D, et al. Ray optics at a deep-sub-wavelength scale: A transformation optics approach. Nano Lett, 2008, 8: 4243–4247
25 Kildishev A, Shalaev V. Engineering space for light via transformation optics. Opt Lett, 2008, 33: 43–45
26 Xiong Y, Liu Z, Zhang X. A simple design of flat hyperlens for lithography and imaging with half-pitch resolution down to 20 nm. Appl Phys Lett, 2009, 94: 203108
27 Smith E, Liu Z, Mei Y, et al. System investigation of a rolled-up metamaterial optical hyperlens structure. Appl Phys Lett, 2009, 95: 083104
28 Smith E J, Liu Z, Mei Y F, et al. Erratum: System investigation of a rolled-up metamaterial optical hyperlens structure. Appl Phys Lett, 2010, 96: 019902
29 Schwaiger S, Bröll M, Krohn A, et al. Rolled-up three-dimensional metamaterials with a tunable plasma frequency in the visible regime. Phys Rev Lett, 2009, 102: 163903
30 Zhang S, Yin L, Fang N. Focusing ultrasound with an acoustic metamaterial network. Phys Rev Lett, 2009, 102: 194301